Chemical Engineering Journal 497 (2024) 154366

Contents lists available at ScienceDirect

Chemical Engineering Journal

journal homepage: www.elsevier.com/locate/cej

3D-printed indium oxide monoliths for PFAS removal

Alysson Stefan Martins [a,1], Garyfalia A. Zoumpouli [a,1], Shan Yi [b], Antonio Jose Exposito [a], Jannis Wenk [a], Davide Mattia [a,*]

[a] Department of Chemical Engineering, University of Bath, Claverton Down, Bath, England BA2 7AY, UK
[b] Department of Chemical and Materials Engineering, The University of Auckland, Auckland 1142, New Zealand

ARTICLE INFO

Keywords:
3D printing
Adsorption
PFAS
PFOA
In_2O_3 catalyst
Self-supported structure

ABSTRACT

More efficient removal methods for per- and polyfluoroalkyl substances (PFAS), anthropogenic compounds with high persistence in the environment, are urgently needed due to their significant adverse health effects. Current technologies for PFAS removal in water are limited by incomplete degradation or practical concerns about the use of slurry-based adsorbents. In this study, self-supported indium oxide (In_2O_3) monoliths were produced via extrusion-based 3D printing and used for the removal of perfluorooctanoic acid (PFOA) via adsorption in a recirculating flow system. A detailed study of the sintering temperature, monolith geometry, and flow rate allowed maximising PFOA adsorption due to the improvement of PFOA diffusion and the increased number of active sites on the monolith, resulting in 53 % of PFOA removal with fast adsorption kinetics in 3 h. Additionally, a low-temperature pyrolysis process at 500 °C effectively regenerated the In_2O_3 monoliths, allowing reusing the monoliths for three adsorption cycles, while also improving the PFOA removal to 75 % in 3 h. The regenerated In_2O_3 monoliths not only have a high adsorption capacity (0.16 mg g^{-1}), but also required a much shorter time to reach the adsorption equilibrium compared with other adsorbents reported in the literature. The effectiveness, robustness and reusability of the 3D printed In_2O_3 monoliths highlight their potential as an efficient and sustainable adsorbent for PFAS removal. The approach presented here represents an effective strategy for the fabrication of complex adsorbents, which are reusable and can be easily handled, eliminating the expensive downstream removal required for slurries while offering a clear route for scale-up towards industrial use.

1. Introduction

Per and polyfluoroalkyl substances (PFAS) are a class of synthetic compounds widely used in various industrial and everyday applications for decades due to their thermal stability, chemical resistance, and relatively high water solubility [1,2]. These properties make PFAS suitable for a diverse range of products including food packaging, fire retardants and waterproof fabrics [3,4].

Among PFAS, perfluorooctanoic acid (PFOA) is one of the most commonly used and recognized compounds, often found as a degradation end product of other PFAS [2,5,6]. Due to their intensive use and chemical stability, PFAS are globally detected in various environmental media, including aquatic and terrestrial ecosystems, and even human blood and breast milk [7–9].

Studies have linked PFAS exposure to various health issues, including reproductive and developmental effects, cardiovascular and cerebrovascular diseases, diabetes, thyroid dysfunction, increased cholesterol, and immune system problems [5]. To mitigate exposure, the U.S. Environmental Protection Agency (EPA) established a lifetime advisory limit of 70 ng/L for combined PFOA and perfluorooctanesulfonic acid (PFOS) in drinking water in 2016 [1,3]. In 2022, the EPA updated the health advisory level for PFOA to a significantly lower value of 0.004 ng/L [10]. Since 2020, the European Union has also banned PFOA in products at concentrations equal to or above 25 ppb or 1000 ppb of related substances [11]. Despite these stringent regulations, PFAS continue to persist in aquatic environments and are resistant toward chemical and biological degradation [4,12–14].

Advanced oxidation processes (AOPs), including photocatalysis [15], electrocatalysis [16,17], sonolysis [18–20], hydrolysis [21], and chemical oxidation [22,23] have shown some efficiency but are either unable to completely degrade PFAS or are too costly for industrial-scale implementation. More recent methods, e.g. combining photo- and

* Corresponding author.
E-mail address: d.mattia@bath.ac.uk (D. Mattia).
[1] These two authors have contributed equally.

https://doi.org/10.1016/j.cej.2024.154366
Received 29 April 2024; Received in revised form 24 July 2024; Accepted 27 July 2024
Available online 28 July 2024

electro-oxidation [24,25], or advanced reduction processes [26] have shown more promise in achieving complete degradation of some PFAS compounds. However, due to the limitations and complexities of direct degradation methods, current PFAS removal strategies primarily rely on sorbents [7,27–29], followed by incineration [30]. Activated carbon is the most commonly used adsorptive material for PFAS removal [28], but it is non-selective for short-chain PFAS governed by physical adsorption [31,32]. Activated carbon's susceptibility to oxidation at elevated temperatures limits its regeneration capacity via thermal desorption, resulting in material loss during incineration [33,34]. Alternative chemical desorption methods require expensive and toxic organic solvents, making them less practicable [27,35].

Inorganic sorbents might be a better alternative for PFAS adsorption due to their high-temperature stability, allowing regeneration via thermal treatment. Although there has been limited research on the adsorption capacity of inorganic compounds to PFAS, studies investigating the photocatalytic degradation of PFAS by metal oxides such as TiO_2, Ga_2O_3 and In_2O_3 provide insights [36,37]. Indium oxide, in particular, has been extensively studied as a photocatalyst for PFAS degradation, showing high removal rates for PFOA [8,36,38–41]. Short pre-adsorption steps (30–60 min) demonstrated significant declines in PFOA concentration, raising questions about whether the observed effects were due to degradation, further adsorption, or a combination of both [42].

Based on these observations and the potential for sorbent regeneration, indium oxide was investigated as a sorbent for PFOA and other short-chain PFAS. Limited literature exists on the adsorptive capacity of In_2O_3 for PFAS, with most studies focusing on adsorption in combination with photocatalysis [43,44]. High removal efficiency is attributed to the tight coordination between the In_2O_3 surface and the terminal carboxylate groups of PFOA (via bidentate or bridging configuration) resulting in a vertical and highly ordered adsorption mode [38,45–47]. One study has showed that using In_2O_3 nanoparticles in slurry reactor achieved about 90 % of PFOA decomposition via adsorption/photocatalysis [44]. Other studies improved the performance of In_2O_3 by increasing the number of active sites through doping, thereby enhancing adsorption capacity [40,48]. However, using nanoparticle slurries is challenging for large-scale applications due to the need for additional steps to prevent nanoparticle leaching [49–51]. To overcome these issues, self-supported structures such as monoliths and foams provide a valid alternative, facilitating sorbent removal while maintaining a high surface area [49].

3D printing has recently emerged as a manufacturing technology that enables the fabrication of hierarchical self-supporting structures, with complex geometries not achievable by other means [52,53]. Printed structures offer advantages such as high structural design freedom, fast fabrication, waste reduction, and cost effectiveness [54].

In this work, free-standing In_2O_3 monoliths were fabricated for the first time using 3D printing by optimizing an indium oxide ink and controlling printing and design parameters. The extrusion-based approach is cost-effective compared to other 3D printing methods as it does not require specialized filaments or resins. The finished structures exhibit minimal shrinkage after thermal treatment, facilitating the development of 3D designs. The 3D printed monoliths demonstrated high adsorption capacity for PFOA in a recirculating flow setup. These monoliths can be regenerated using a low-temperature pyrolysis process, maintaining or even increasing their PFOA sorption capacity, showcasing their potential for reuse after adsorption-regeneration cycles.

2. Materials and methods

2.1. Materials

High purity In_2O_3 powder (99.99 % – D50 < 2.06um) was acquired from Xi'An Function Material Group Co. (China). The surfactant Pluronic F-127 was purchased from Merck. The solvents methanol, ethanol (Absolute) and acetonitrile were purchased from VWR and used as provided. Perfluorooctanoic acid, used here as a target organic pollutant, and ammonium acetate were supplied by Sigma-Aldrich. The native analytical standard of PFOA and the corresponding stable-isotope-labelled internal standard used for quantification were purchased from Greyhound Chromatography. All solutions were prepared from ultrapure water (Veolia Purelab Chorus, 18.2 MΩ).

2.2. Preparation of 3d printing ink

The ink used in the extrusion-based 3D printing was prepared by dispersing In_2O_3 powder (D50 $\leq$ 2.1 μm) in a Pluronic F-127 solution (15 % v/v), which was used as a binder, at room temperature (25 °C) under constant and vigorous physical mixing for ~ 15 min. Once the mixture became a well-incorporated and homogenous ink, it was directly loaded into the printer's cartridge which, in turn, was then connected to the 3D-printer (VormVrij|3D Lutum®5). The extrusion, speed factor, and pressure parameters were critical for the 3D printing process and were optimised to achieve high quality and reproducible printing.

Monolith designs were made with the Prusa Slicer software and subsequently exported to generate SLA files converted to G-Code commands. The printed designs were patterned layer by layer (rods of 1.2 mm) in a cylindrical scaffold structure (20 mm Ø) with a rectilinear pattern and initial length of 20 mm. The open porosity corresponded to 70 %, adapted to the dimensions of the recirculating flow setup used in the sorption tests. This geometry was designed to maximize the surface area, which improves the exposure of active sites, and the flow of the pollutant solution permeating through it, translating into rapid mass transfer, while minimizing pressure drop [55]. After being printed, the monoliths were dried at room temperature for 12 h and subsequently sintered at 500 °C for 10 h in air in a tubular furnace with a heating rate of 5 °C/min and a cooling rate of 3 °C/min. The shrinkage of the structure was less than 5 % after sintering.

2.3. Characterization

The surface characterization was performed using field emission scanning electron microscopy (JEOL JSM-7900F FESEM), with the samples coated with 20 nm Cr. The particle size distribution was calculated using ImageJ software. The crystal structure of the monoliths was investigated by X-ray Diffraction (XRD), carried out with a STOE STADI P dual powder transmission X-ray diffractometer, using Cu Kα1 radiation with a wavelength of 1.54 Å, and a 2θ scan from 20 to 90° with a period of 20 min. The surface area was estimated using Brunauer – Emmett – Teller (BET) calculations carried out with nitrogen adsorption – desorption measurements using Autosorb-iQ-C by Quantachrome Anton Paar at 77 K, after degassing under vacuum at 120 °C for 120 min. Raman spectra were collected using a Renishaw InVia Confocal Raman microscope, with an excitation laser wavelength of 532 nm. Thermogravimetric analysis was conducted using a Setaram Setsys Evo under nitrogen atmosphere with a heating rate of 10 °C/min up to 950 °C. The compressive strength of the In_2O_3 monolith was measured using an Instron 3365 testing machine equipped with a 2 KN sensor. The crosshead speed was set to 0.5 mm/min in the displacement control mode until the sample fracture was detected in the force displacement plot.

2.4. Flow setup and PFOA removal

The PFOA removal was studied using a recirculating flow setup, as schematically represented in **Fig. S1**. The In_2O_3 monolith (length of 21 or 44 mm and mass of 5.5 or 10 g, respectively) was placed inside a quartz tube, and a recirculating water-cooling system was connected to the 500 ml setup with a constant temperature of 10 °C. The initial concentration of PFOA was set to 10 μM (4.1 mg L^{-1}). The solution pH was measured as 6.6 and not adjusted further. The solution flowed

through the quartz tube containing the monolith using a pulseless gear pump (MCP-Z Ismatec) operating from 100 to 700 mL min^{-1} for 180 min. All tubing used was non-fluorinated silicone (Masterflex™ L/S™, Platinum-Cured Silicone). After a predetermined time, 3.0 mL of PFOA solution was collected using a disposable syringe and filtered using a 0.20 μm fluorine-free filter (regenerated cellulose, Agilent, UK) into a polypropylene vial to remove any residual particles. The total volume removed by sampling was less than 5 % of the total volume flowing in the setup. The PFOA studies were conducted in duplicate. The first 1.5 mL of filtrate were discarded to prevent potential interference from PFOA adsorption by the filter.

2.5. PFOA analysis

PFOA was quantified using high-performance liquid chromatography coupled with a single quadrupole mass spectrometry (HPLC-MS) with an Agilent 1260 Infinity II (Quaternary Pump). An Agilent PFC-Free HPLC Conversion Kit and an InfinityLab PFC delay column (4.6 x 30 mm) were installed to minimise background PFOA levels. Chromatographic separation was performed with a RRHD Eclipse Plus C18 reverse phase column (2.1 x 100 mm, particle size 1.8 μm), including an Eclipse Plus C18 Guard column (2.1 x 5 mm, particle size 1.8 μm). The column temperature was set to 50 °C. The mobile phase consisted of 5 mM ammonium acetate in ultrapure water (A) and 5 mM ammonium acetate in methanol (B). Gradient elution was used starting with 95 % A for 1 min, decreasing linearly to 45 % A at 4 min and then to 10 % A at 9 min, keeping 10 % A for 5 min, then returning to 95 % A with a 21 min stop time, at a flow rate of 0.35 mL min^{-1}. The injection volume was 5 μL. Selected ion monitoring (SIM) mode was used to maximize the instrument performance. The mass spectrometer was equipped with an electrospray ionization (ESI) source, operating in the negative ion mode with a capillary voltage of −2500 eV, 25 psi N_2 nebulizer gas at a flow of 11 L min^{-1}, N_2 collision gas, a temperature of 325 °C and a nozzle voltage of 500 V. The ion detected for PFOA was *m/z* 413, and its internal standard was *m/z* 421. Each sample was spiked with the internal standard after filtration and was injected in triplicate. The linear range of the PFOA calibration curve was 0.0025 to 4.5 mg L^{-1}, with a detection limit of 0.001 mg L^{-1}. The removal of PFOA via adsorption was measured by plotting $[C]/[C_0]$ vs. time and the adsorption kinetic was calculated by linear regression of a plot of $(\ln([C]/[C_0]))$ vs. time. The adsorption capacity of PFOA onto In_2O_3 was estimated by the following equation [56,57]:

$q_e = (C_0 - C_e) \times V/M$ (1).

where q_e is the equilibrium adsorption capacity (mg g^{-1}), C_0 is the initial concentration of PFOA (mg L^{-1}), C_e is the residual concentration of PFOA (mg/L), V is the volume of the solution (L), and M is the mass of In_2O_3 monolith (g).

2.6. Pyrolysis process

A tubular muffle oven (Carbolite CWF 1100) was used as a pyrolysis reactor to study the regeneration of the monoliths. The 3D printed structures were inserted centrally into a stainless-steel tube (25 mm in diameter and 70 cm in length) located inside the furnace and connected with a N_2 gas source. The outlet gas was connected to an apparatus composed of two condensers in series. The first condenser was placed in a recirculating water-cooling system, while the second went through a saturated NaOH solution, which collected and concentrated gaseous products generated during the heating process. The system was purged with N_2 for 30 min at a flow rate of 300 mL min^{-1}, and subsequently heated at 500 °C for a fixed residence time of 120 min. Subsequently, the monolith was left to rest for 60 min and carefully removed from the reactor.

3. Results and discussion

3.1. Monolith synthesis and characterization

The fabrication of In_2O_3 monoliths via 3D printer extrusion required the development of a novel ink formulation combining In_2O_3 powder with an aqueous solution containing 15 wt% of the polymeric binder Pluronic F127. The optimized formulation, with 86 wt% of solid content, combined with the precise control of printer parameters allowed a direct printing of 3D structures through layer-by-layer without the need for additional solidification treatments, making this technique suitable for scale-up fabrication. For inks with lower solid content, the printability process was significantly compromised, exhibiting low viscosity which resulted into a sagging scaffold structure and poor shape retention. In contrast, ink with In_2O_3 content higher than 86 wt% was too thick to be extruded from the nozzle, requiring excessive pressure (≥6 bar) and making the printing process impractical.

As shown in Fig. 1**A**, the optimized formulation enabled printing of a self-supporting cylindrical structures using a continuous fine filament (1.2 mm), producing up to 15 different monoliths in a single ink batch (200 g), as shown in Fig. 1**B**. Monoliths of different lenghts can be produced with this approach, with 12, 18, and 25 layers, measuring 21, 35 and 44 mm high, respectively (Fig. 1**C**). All the monoliths retained the millimetre-sized mesh opening structures, resulting in an ideal design for flow systems, where the abundant gaps enable good mixing with minimal pressure loss.

The effect of the temperature on the sintering process of the In_2O_3 monoliths was investigated at 500, 700, 900, and 1,100 °C for 10 h in air. The volume shrinkage of the 3D structures was less than 5 % after sintering for all temperature conditions, retaining the original design, including the open mesh structure. Thermogravimetric analysis (TGA) was used to determine the thermal degradation of the F127 binder (**Fig. S2**) and revealed that the compound was completely removed/decomposed from the In_2O_3 monoliths for temperatures above 450 °C. Raman analysis also confirmed the absence of any residual carbon in the In_2O_3 monoliths after the F127 binder decomposition (**Fig. S3**).

The surface of the printed object prior to sintering showed an agglomeration of the initial indium oxide powder into cuboidal structures with a rough and irregular surface (Fig. 2**-left panel**). The subsequent sintering led not only to the fusion of the particles in a continuous, interconnected structure (Fig. 2**-centre and right panels**), but also the growth of particle size with increasing sintering temperature (Fig. 3**A**). The monoliths sintered at higher temperatures also possessed smoother microstructures, with less irregularity, which may affect the surface area and consequently the adsorption performance of the In_2O_3 monolith (**Fig. S4**).

The XRD patterns of the monoliths showed no obvious change with the sintering temperature (Fig. 3**B**), with the XRD pattern corresponding to cubic In_2O_3 in agreement with reported data from JCPDS No. 06–0416 [38,41]. The N_2 adsorption/desorption isotherms (Fig. 3**C**) and the BET analysis showed no significant differences following sintering, with surface area values of 11.74, 8.49, and 6.68 m^2 g^{-1} for the as-received In_2O_3 powder, and the samples sintered at 500 and 1,100 °C, respectively. In general, materials with large BET specific surface areas possess high physical adsorption, which is primarily governed by nonselective interactions between the adsorbate molecules and the material's surface [42], while chemical adsorption is not directly correlated with the specific surface area. This outcome suggests that the adsorption mechanism of PFOA on the In_2O_3 surface is likely to be associated with chemical adsorption, specifically dominated by active sites, rather than physical adsorption. Furthermore, it is well known that only In^{3+} ions in In_2O_3 can effectively coordinate with the carboxyl group of PFOA [46,58], and that the saturation of In^{3+} is affected by the sintering process [46,58].

The monoliths were subjected to compression tests up to failure (Fig. 3**D**). As expected, the printed object prior to sintering is

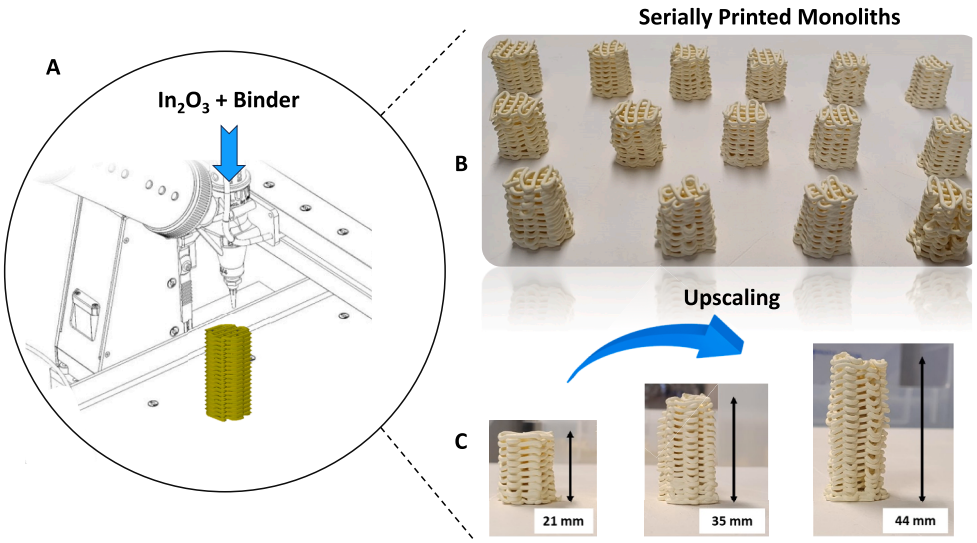

Fig. 1. (A) schematic representation of 3D printer extrusion, (B) successively produced In_2O_3 monolithic structures, and (C) upscaling of In_2O_3 monoliths.

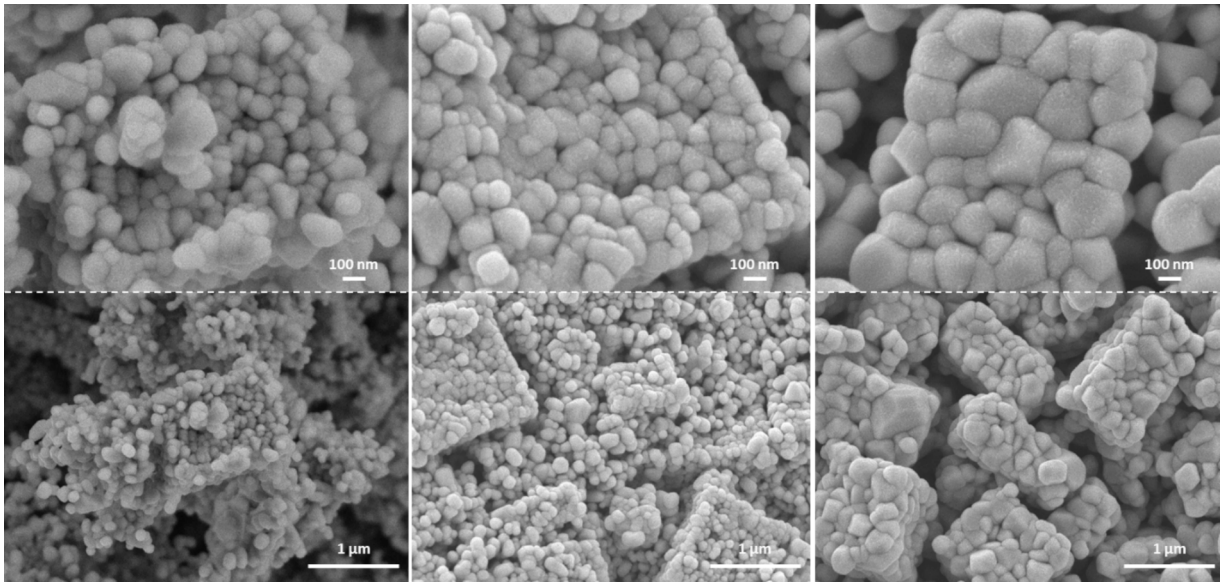

Fig. 2. FESEM micrographs of In_2O_3 monoliths as prepared (left) and after sintering at 500 (centre) and 1,100 °C (right).

particularly deformable, exhibiting a linear elastic behaviour up to fracture. In contrast, the monolith sintered at the highest temperature (1,100 °C), broke only at a high stress level, in agreement with the higher density observed in SEM micrographs. Small load drops in the curve for the monolith sintered at 1,100 °C were the result of fragments breaking off the structure. The monolith sintered at 500 °C had sufficient mechanical resistance to compression to be used in a recirculating flow setup.

3.2. PFOA adsorption by 3D printed In_2O_3 monoliths

The adsorption capacity of the 3D-printed In_2O_3 monoliths, sintered at different temperatures, was tested in a recirculating flow setup at a controlled temperature of 10 °C. (Fig. 4**A**). Note that control experiments showed negligible PFOA losses due to adsorption in the flow setup in the absence of a monolith (<5% removal). At an initial flow rate of 300 mL min^{-1}, the monoliths sintered at 500 °C removed 27 % of PFOA after 3 h, with a good first order fitting and a high kinetic constant (Table 1). The sorption occurred despite a low specific surface area (Fig. 3**C**), confirming that this is due to a chemical interaction between the active sites on the surface of the In_2O_3 monolith and PFOA. However, the adsorption removal for PFOA gradually decreased with increasing sintering temperature, along with a slowdown in kinetics with sintering temperature increasing from 500 to 1,100 °C. No significant adsorption of PFOA was observed for the monolith sintered at 1,100 °C, while about 12 % and 21 % adsorption were achieved for the monoliths sintered at 700 °C and 900 °C, respectively. These results agree with observations in the literature that oxygen vacancies on the surface of indium oxide catalysts are reduced by high-temperature treatments [42,58]. The monoliths were weighed before and after each experiment with no change in the monolith mass measured.

It is worth noting that the adsorption–desorption did not achieve equilibrium for the PFOA removal by the end of the experiment, suggesting that there is still a significant potential for the PFOA to be removed via adsorption. Therefore, when the fresh In_2O_3-500 °C monolith was submitted to a longer experiment, the equilibrium adsorption–desorption seemed to have been achieved after 8 h, with about 60 % PFOA removal (Fig. 4**B**). In contrast, the monolith annealed

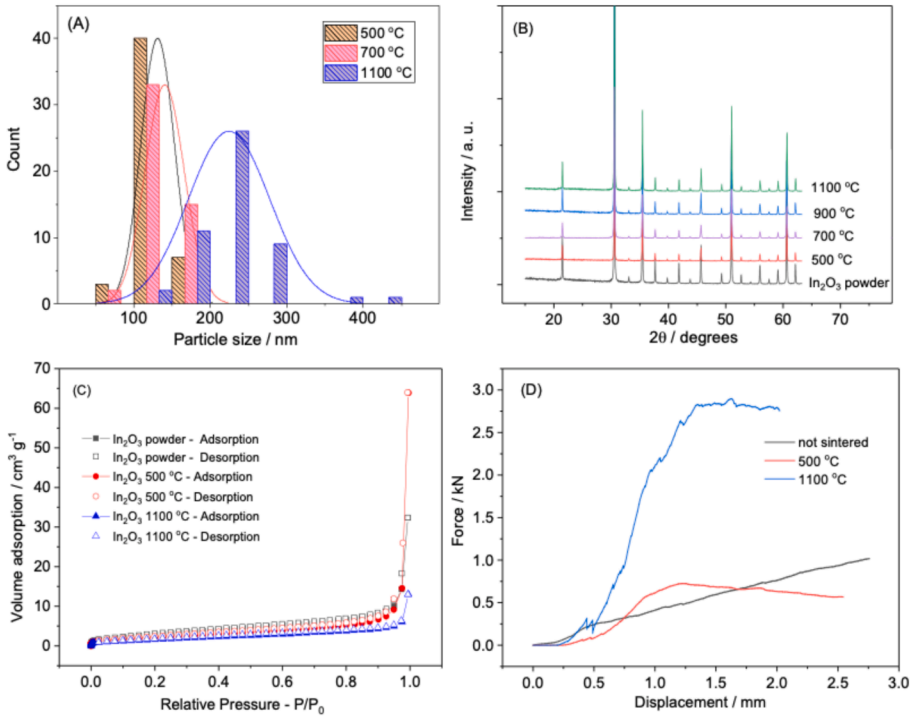

Fig. 3. (A) Overall particle size distribution; (B) XRD pattern; (C) N_2 adsorption–desorption isotherms and (D) compressive stress versus strain responses for In_2O_3 monolith sintered at different temperatures.

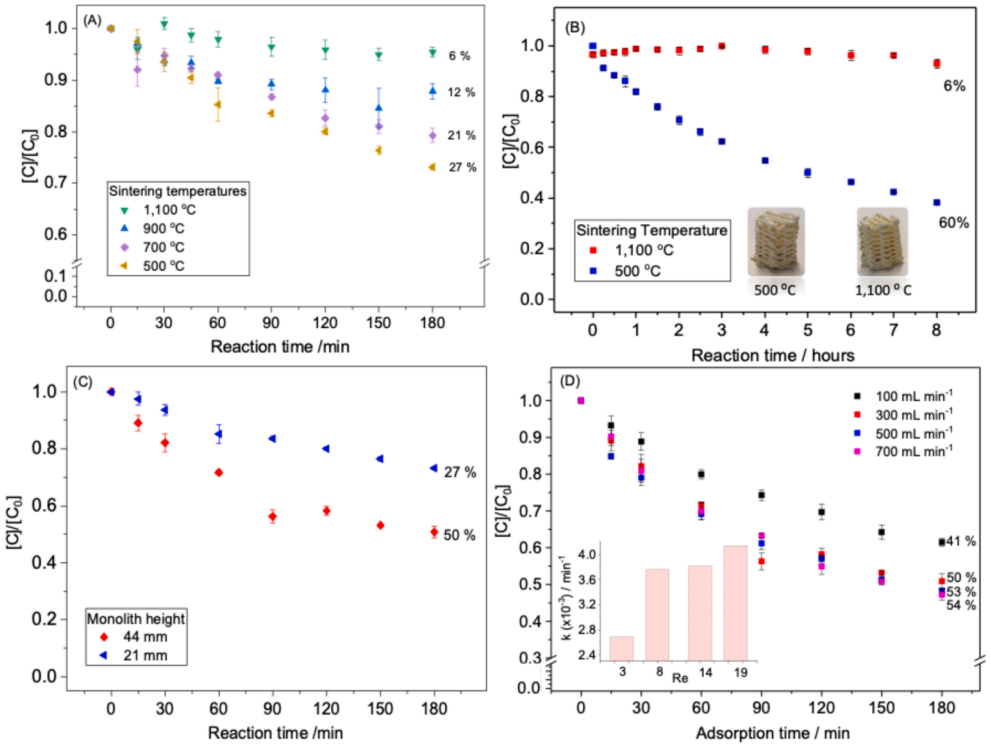

Fig. 4. PFOA adsorption on In_2O_3 monoliths (A) sintered at different temperatures (Condition: Flow rate: 300 mL min^{-1}, monolith length: 21 mm); (B) long experiment (Condition: Flow rate: 300 mL min^{-1}, monolith length: 21 mm); (C) effect of monolith length (Condition: Flow rate: 300 mL min^{-1}); and (D) effect of flow rate (monolith length: 44 mm). The inset shows the kinetics vs. Reynolds number. [PFOA]: 10 μM in all cases.

at 1,100 °C did not show any increase in adsorption for the same period. Therefore, further tests were conducted on monoliths sintered at 500 °C, providing the best combination of adsorption capacity and mechanical stability.

Table 1
PFOA removal and pseudo first order adsorption kinetics (k) for In_2O_3 monoliths evaluated at different sintering temperatures, flow rates, monolith lengths, and regeneration.

	Sintering Temperature (ºC)	Flow Rate (mL min^{-1})	Monolith Length (mm)	PFOA removal (%)	k ($x10^{-3}$ min^{-1}) [R^2]
Fresh Monolith	500	300	21	27	1.7 [0.97]
	700			21	1.2 [0.94]
	900			12	0.8 [0.80]
	1,100			6	–
Fresh Monolith	500	100	44	41	2.7 [0.98]
		300		50	3.8 [0.92]
		500		53	3.8 [0.96]
		700		54	4.1 [0.98]
1st Regeneration	500	500	44	75	7.6 [0.97]
2nd Regeneration				70	6.6 [0.96]

3.3. Operational and structural parameters: Monolith length and flow rate effect

Based on the initial set of results, both the design of the monoliths and the experimental parameters were varied to increase the overall adsorption of PFOA. First, doubling the length of the monoliths – while preserving all other structural parameters – led to a doubling of PFOA adsorption to 50 % (Fig. 4**C**), for the same flowrate (Table 1) and time. The increase in the PFOA removal for the longer structures can be attributed to a proportional increase in the number of active sites across the 3D printed monolith, promoting an improvement of adsorption performance. This is further confirmed by comparing the ratio between the mass of the monolith and the PFOA removal rate, which are 4.9 and 5.0 for the shorter and longer structures, respectively.

Increasing the flow rate from 100 to 500 mL min^{-1} using the longer monolith led to an increase in the adsorption rate, achieving 53 % of removal after 3 h of treatment (Fig. 4**D**), and faster kinetics (Table 1). Such improvement is consequence of an improvement in the convective mass transfer within the flow setup and therefore, a decrease in the thickness of the boundary layer [59], contributing to the diffusion of PFOA on the surface and the subsequent adsorption. The **inset** of Fig. 4**D** shows the kinetics for each flow rate as a function of the Reynolds number and confirms the improvement in mass transfer followed by stabilization above 500 mL^{-1}, typical of a mass transfer-limited regime [55,59]. The monoliths maintained their mechanical integrity for all flow rates tested.

Finally, combining longer experiments at a flow rate of 500 mL min^{-1}, with a 44 mm long monolith (sintered at 500 °C), removal of PFOA reached 67 %, with a high adsorption capacity of 0.14 mg L^{-1} (Fig. 5**S**). These results clearly show that the monolith length combined with flow rate can result in an effective improvement of adsorption capacity, enabling the scale up the 3D designs without compromising the macroscopic integrity.

A comparison between the 3D printed In_2O_3 monoliths prepared here with other PFOA adsorbents is shown Table 2. Notably, carbon-based materials display higher adsorption capacity, which is often associated to their high surface area and porosity, which is primarily governed by physical adsorption. However, it is worth noting that their equilibrium usually requires a longer period, and their use is limited to packed bed or slurry system configurations. According to the literature, the sorption of PFOA in the carbon-based materials is mainly governed by hydrophobic/hydrophilic and electrostatic interactions [60]. In contrast, non-carbon adsorbents also have an additional contribution from chemical adsorption, where the number of binding sites plays a vital role on the degree of adsorption [61].

The 3D printed In_2O_3 monoliths outperform non-carbon-based absorbents such as TiO_2 and alumina by 2 to 10 orders of magnitude, reaching apparent equilibrium after 8 h (Table 2). This highlights the benefits of adsorption coordination of In_2O_3 with PFOA which, associated with the self-supported 3D structures, could result in lower treatment costs and fewer steps related to the separation of the adsorbents. It is further noted that most of the studies on PFOA removal used slurry systems and batch configurations, which are not suitable for practical use.

3.4. Regeneration and reuse of In_2O_3 monoliths for adsorption of PFOA

Although the In_2O_3 monoliths have demonstrated a high adsorption capacity for PFOA and good mechanical robustness in flow, in terms of applicability, it is crucial to assess the regeneration capability of the

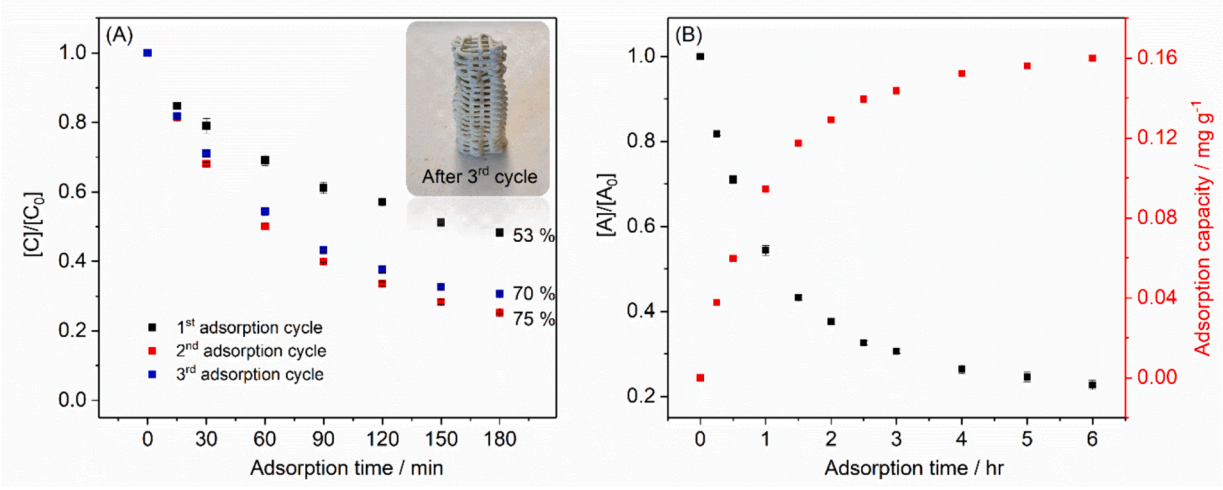

Fig. 5. PFOA adsorption on (A) a new In_2O_3 monolith and after regeneration by pyrolysis, (B) submitted to a long experiment after pyrolysis. Conditions: Flow rate: 500 mL min^{-1}, and [PFOA]: 10 μM, monolith length: 44 mm.

Table 2
Comparison of adsorption capacity of In_2O_3 monolith with other reported adsorbents.

Material	Adsorbent	System	$[PFOA]_0$ (mg L^{-1})	Equilibrium Time (h)	Adsorption Capacity (mg g^{-1})	Ref
Carbon Based	Suspension (g/L)	Batch (mL)				
Activated Carbon/Fe^0	1.0	50	10	240	30.1	[62]
Mesoporous Carbon	0.05	200	10	5	29.6	[56]
PEI modified cellulose	0.05	250	0.1	2	2.32	[63]
GO $ZnFe_3O_4$/ Chitosan	1.0	10	20	15	21.64	[57]
MIP adsorbent	0.2	50	0.02	48	5.45	[64]
Carbon nanotubes	0.25 g	40	0.083	25	0.187	[60]
Non-carbon based	Suspension (g/L)	Batch (mL)				
Alumina	10.0	20	0.1	48	0.014	[65]
AlO(OH)	5.0	20	0.2	48	0.189	[66]
TiO_2/graphene	0.02	200	5.0	0.15	0.026	[67]
Fe-AlOx/Fe-AlOHx	10.0	600	1	24	0.097	[61]
TiO_2/MOF	0.02	200	4.14	0.15	0.076	[68]
	Self-supported (g)	Recirculating (mL)				
In_2O_3 New	10	500	4.14	8	0.14	This work
1st Reg.					0.16	

adsorbent material. Taking this into consideration, a low temperature (500 °C) pyrolysis process was used to regenerate the In_2O_3 monoliths after adsorption. Somewhat surprisingly, after the first regeneration, the monoliths substantially increased the removal of PFOA to about 75 % for only three hours of treatment (Fig. 5**A**), resulting in the highest kinetics of 0.0076 min^{-1} (Table 1). After 6 h of experiment, the regenerated monolith had an adsorption capacity of 0.16 mg g^{-1} (Fig. 5**B**), higher than most non-carbon sorbents in the literature (Table 2). This might be associated with an increase in the number of active sites following the pyrolysis treatment at 500 °C in addition to the desorption of the PFOA molecules from the surface [69].

After the second regeneration, removal decreased to about 70 % of PFOA (Fig. 5**A**), possibly related to microscopic material losses. Note, the mass change of each monolith during pyrolysis was less than 5 %. However, as shown in the optical image of Fig. 5**A**, there are no structural changes nor visible losses of material over three cycles of regeneration-adsorption, confirming the robustness of the monoliths. The reusability of the developed monoliths after a low-temperature pyrolysis process implies that their practical implementation would be cost-effective despite the relatively high initial cost of the indium oxide material.

4. Conclusion

This study successfully demonstrated the fabrication of self-supported In_2O_3 monoliths using an extrusion-based 3D printing technique. The monoliths exhibit excellent mechanical stability and a high adsorption capacity for PFOA, even with a relatively low specific surface area. The influence of sintering temperature, monolith length, and flow rate on the adsorption performance was systematically explored, allowing for the optimization of In_2O_3 monoliths removing up to 75 % of PFOA, with a high adsorption capacity (0.16 mg g^{-1}). The monoliths could be efficiently regenerated through a low-temperature pyrolysis process, which resulted in an increased adsorption capacity over 3 regeneration-adsorption cycles. The low-cost 3D printing fabrication, low-temperature regeneration process, and reusability of the In_2O_3 monoliths suggest they have the potential to be a cost-effective alternative for the removal of PFAS from contaminated water sources. This study represents a significant step toward the development of practical and efficient solutions for mitigating the environmental impact of PFAS contamination, offering an environmentally sustainable and effective solution for PFAS remediation.

CRediT authorship contribution statement

Alysson Stefan Martins: . **Garyfalia A. Zoumpouli:** Writing – original draft, Methodology, Investigation, Formal analysis. **Shan Yi:** Validation, Formal analysis. **Antonio Jose Exposito:** . **Jannis Wenk:** Writing – review & editing, Supervision, Formal analysis. **Davide Mattia:** Writing – review & editing, Resources, Project administration, Methodology, Funding acquisition, Conceptualization.

Declaration of competing interest

The authors declare that they have no known competing financial interests or personal relationships that could have appeared to influence the work reported in this paper.

Data availability

data access statement present at end of manuscript

Acknowledgment

Funding: This work was supported by the UK EPSRC [grant numbers EP/P031382/1 and EP/V047078/1]. We are also grateful to Mr. Paul Frith for the technical support on the flow setup design. All data produced during this research are available from the University of Bath open access data archive at https://doi.org/10.15125/BATH-01410.

Appendix A. Supplementary data

Supplementary data to this article can be found online at https://doi.org/10.1016/j.cej.2024.154366.

References

[1] S.C.E. Leung, P. Shukla, D. Chen, E. Eftekhari, H. An, F. Zare, N. Ghasemi, D. Zhang, N.T. Nguyen, Q. Li, Emerging technologies for PFOS/PFOA degradation and removal: a review, Sci. Total Environ. 827 (2022) 153669, https://doi.org/10.1016/j.scitotenv.2022.153669.
[2] K.H. Kucharzyk, R. Darlington, M. Benotti, R. Deeb, E. Hawley, Novel treatment technologies for PFAS compounds: a critical review, J. Environ. Manage. 204 (Pt 2) (2017) 757–764, https://doi.org/10.1016/j.jenvman.2017.08.016.
[3] R.A. Dickman, D.S. Aga, A review of recent studies on toxicity, sequestration, and degradation of per- and polyfluoroalkyl substances (PFAS), J. Hazard. Mater. 436 (2022) 129120, https://doi.org/10.1016/j.jhazmat.2022.129120.
[4] X. Liu, W. Wei, J. Xu, D. Wang, L. Song, B.J. Ni, Photochemical decomposition of perfluorochemicals in contaminated water, Water Res. 186 (2020) 116311, https://doi.org/10.1016/j.watres.2020.116311.
[5] S. Yadav, I. Ibrar, R.A. Al-Juboori, L. Singh, N. Ganbat, T. Kazwini, E. Karbassiyazdi, A.K. Samal, S. Subbiah, A. Altaee, Updated review on emerging technologies for PFAS contaminated water treatment, Chem. Eng. Res. Des. 182 (2022) 667–700, https://doi.org/10.1016/j.cherd.2022.04.009.
[6] J.N. Meegoda, B. Bezerra de Souza, M.M. Casarini, J.A. Kewalramani, A Review of PFAS Destruction Technologies, Int. J. Environ. Res. Public Health 19 (24) (2022), https://doi.org/10.3390/ijerph192416397.
[7] Y. Qi, H. Cao, W. Pan, C. Wang, Y. Liang, The role of dissolved organic matter during Per- and Polyfluorinated Substance (PFAS) adsorption, degradation, and

plant uptake: a review, J. Hazard. Mater. 436 (2022) 129139, https://doi.org/10.1016/j.jhazmat.2022.129139.
[8] J. Liu, C. Guo, N. Wu, C. Li, R. Qu, Z. Wang, R. Jin, Y. Qiao, Z. He, J. Lu, X. Feng, Y. Zhang, A. Wang, J. Gao, Efficient photocatalytic degradation of PFOA in N-doped In2O3/simulated sunlight irradiation system and its mechanism, Chem. Eng. J. 435 (2022), https://doi.org/10.1016/j.cej.2022.134627.
[9] N. Kotlarz, J. McCord, D. Collier, C.S. Lea, M. Strynar, A.B. Lindstrom, A.A. Wilkie, J.Y. Islam, K. Matney, P. Tarte, M.E. Polera, K. Burdette, J. DeWitt, K. May, R. C. Smart, D.R.U. Knappe, J.A. Hoppin, Measurement of Novel, Drinking Water-Associated PFAS in Blood from Adults and Children in Wilmington, North Carolina, Environ. Health Perspect. 128 (7) (2020) 77005, https://doi.org/10.1289/EHP6837.
[10] X. Chen, J. Li, L. Han, W. Wu, M. Chen, Human health risk-based soil generic assessment criteria of representative perfluoroalkyl acids (PFAAs) under the agricultural land use in typical Chinese regions, Environ. Pollut. 335 (2023) 122368, https://doi.org/10.1016/j.envpol.2023.122368.
[11] M.A. Uriakhil, T. Sidnell, A. De Castro Fernandez, J. Lee, I. Ross, M. Bussemaker, Per- and poly-fluoroalkyl substance remediation from soil and sorbents: a review of adsorption behaviour and ultrasonic treatment, Chemosphere 282 (2021) 131025, https://doi.org/10.1016/j.chemosphere.2021.131025.
[12] X. Bai, Y. Son, Perfluoroalkyl substances (PFAS) in surface water and sediments from two urban watersheds in Nevada, USA, Sci Total Environ 751 (2021) 141622, https://doi.org/10.1016/j.scitotenv.2020.141622.
[13] S. Kurwadkar, J. Dane, S.R. Kanel, M.N. Nadagouda, R.W. Cawdrey, B. Ambade, G. C. Struckhoff, R. Wilkin, Per- and polyfluoroalkyl substances in water and wastewater: a critical review of their global occurrence and distribution, Sci. Total Environ. 809 (2022) 151003, https://doi.org/10.1016/j.scitotenv.2021.151003.
[14] S.J. Chow, N. Ojeda, J.G. Jacangelo, K.J. Schwab, Detection of ultrashort-chain and other per- and polyfluoroalkyl substances (PFAS) in U.S. bottled water, Water Res. 201 (2021) 117292, https://doi.org/10.1016/j.watres.2021.117292.
[15] J. Gao, Z. Liu, Z. Chen, D. Rao, S. Che, C. Gu, Y. Men, J. Huang, J. Liu, Photochemical degradation pathways and near-complete defluorination of chlorinated polyfluoroalkyl substances, Nature Water 1 (4) (2023) 381–390, https://doi.org/10.1038/s44221-023-00046-z.
[16] J. Radjenovic, N. Duinslaeger, S.S. Avval, B.P. Chaplin, Facing the challenge of poly- and perfluoroalkyl substances in water: is electrochemical oxidation the answer? Environ. Sci. Tech. 54 (23) (2020) 14815–14829, https://doi.org/10.1021/acs.est.0c06212.
[17] N. Duinslaeger, J. Radjenovic, Electrochemical degradation of per- and polyfluoroalkyl substances (PFAS) using low-cost graphene sponge electrodes, Water Res. 213 (2022) 118148, https://doi.org/10.1016/j.watres.2022.118148.
[18] W. Zhang, Q. Zhang, Y. Liang, Ineffectiveness of ultrasound at low frequency for treating per- and polyfluoroalkyl substances in sewage sludge, Chemosphere 286 (Pt 2) (2022) 131748, https://doi.org/10.1016/j.chemosphere.2021.131748.
[19] B. Bezerra de Souza, S. Aluthgun Hewage, J.A. Kewalramani, A. Ct van Duin, J. N. Meegoda, A ReaxFF-based molecular dynamics study of the destruction of PFAS due to ultrasound, Environ. Pollut. 333 (2023) 122026, https://doi.org/10.1016/j.envpol.2023.122026.
[20] J.A. Kewalramani, B. Wang, R.W. Marsh, J.N. Meegoda, L. Rodriguez Freire, Coupled high and low-frequency ultrasound remediation of PFAS-contaminated soils, Ultrason. Sonochem. 88 (2022) 106063, https://doi.org/10.1016/j.ultsonch.2022.106063.
[21] B.N. Nzeribe, M. Crimi, S. Mededovic Thagard, T.m., Holsen, Physico-Chemical Processes for the Treatment of Per- And Polyfluoroalkyl Substances (PFAS): a review, Crit. Rev. Environ. Sci. Technol. 49 (10) (2019) 866–915, https://doi.org/10.1080/10643389.2018.1542916.
[22] Y. Deng, Z. Liang, X. Lu, D. Chen, Z. Li, F. Wang, The degradation mechanisms of perfluorooctanoic acid (PFOA) and perfluorooctane sulfonic acid (PFOS) by different chemical methods: a critical review, Chemosphere 283 (2021) 131168, https://doi.org/10.1016/j.chemosphere.2021.131168.
[23] C. Berg, B. Crone, B. Gullett, M. Higuchi, M.J. Krause, P.M. Lemieux, T. Martin, E. P. Shields, E. Struble, E. Thoma, A. Whitehill, Developing innovative treatment technologies for PFAS-containing wastes, J. Air Waste Manag. Assoc. 72 (6) (2022) 540–555, https://doi.org/10.1080/10962247.2021.2000903.
[24] E. Banayan Esfahani, F. Asadi Zeidabadi, M. Jafarikojour, M. Mohseni, Photo-oxidative/reductive decomposition of perfluorooctanoic acid (PFOA) and its common alternatives: mechanism and kinetic modeling, J. Water Process Eng. 61 (2024) 105332, https://doi.org/10.1016/j.jwpe.2024.105332.
[25] Y. Guan, Z. Liu, N. Yang, S. Yang, L.E. Quispe-Cardenas, J. Liu, Y. Yang, Near-complete destruction of PFAS in aqueous film-forming foam by integrated photo-electrochemical processes, Nature Water 2 (5) (2024) 443–452, https://doi.org/10.1038/s44221-024-00232-7.
[26] L. Saleh, M. Remot, Q.B. Remaury, P. Pardon, P. Labadi, H. Budzinski, C. Coutanceau, J.-P. Croué, PFAS degradation by anodic electrooxidation: influence of BDD electrode configuration and presence of dissolved organic matter, Chem. Eng. J. 489 (2024) 151355, https://doi.org/10.1016/j.cej.2024.151355.
[27] F. Li, Z. Wei, K. He, L. Blaney, X. Cheng, T. Xu, W. Liu, D. Zhao, A concentrate-and-destroy technique for degradation of perfluorooctanoic acid in water using a new adsorptive photocatalyst, Water Res. 185 (2020) 116219, https://doi.org/10.1016/j.watres.2020.116219.
[28] P.S. Pauletto, T.J. Bandosz, Activated carbon versus metal-organic frameworks: a review of their PFAS adsorption performance, J. Hazard. Mater. 425 (2022) 127810, https://doi.org/10.1016/j.jhazmat.2021.127810.
[29] S.J. Chow, H.C. Croll, N. Ojeda, J. Klamerus, R. Capelle, J. Oppenheimer, J. G. Jacangelo, K.J. Schwab, C. Prasse, Comparative investigation of PFAS adsorption onto activated carbon and anion exchange resins during long-term operation of a pilot treatment plant, Water Res. 226 (2022) 119198, https://doi.org/10.1016/j.watres.2022.119198.
[30] H.M. Solo-Gabriele, A.S. Jones, A.B. Lindstrom, J.R. Lang, Waste type, incineration, and aeration are associated with per- and polyfluoroalkyl levels in landfill leachates, Waste Manag. 107 (2020) 191–200, https://doi.org/10.1016/j.wasman.2020.03.034.
[31] D. Tian, D. Geng, W. Tyler Mehler, G. Goss, T. Wang, S. Yang, Y. Niu, Y. Zheng, Y. Zhang, Removal of perfluorooctanoic acid (PFOA) from aqueous solution by amino-functionalized graphene oxide (AGO) aerogels: influencing factors, kinetics, isotherms, and thermodynamic studies, Sci Total Environ 783 (2021) 147041, https://doi.org/10.1016/j.scitotenv.2021.147041.
[32] M. Park, S. Wu, I.J. Lopez, J.Y. Chang, T. Karanfil, S.A. Snyder, Adsorption of perfluoroalkyl substances (PFAS) in groundwater by granular activated carbons: roles of hydrophobicity of PFAS and carbon characteristics, Water Res. 170 (2020) 115364, https://doi.org/10.1016/j.watres.2019.115364.
[33] F. Xiao, P.C. Sasi, B. Yao, A. Kubátová, S.A. Golovko, M.Y. Golovko, D. Soli, Thermal Stability and Decomposition of Perfluoroalkyl Substances on Spent Granular Activated Carbon, Environ. Sci. Technol. Lett. 7 (5) (2020) 343–350, https://doi.org/10.1021/acs.estlett.0c00114.
[34] T. Fujimori, A. Toda, K. Mukai, M. Takaoka, Incineration of carbon nanomaterials with sodium chloride as a potential source of PCDD/Fs and PCBs, J. Hazard. Mater. 382 (2020) 121030, https://doi.org/10.1016/j.jhazmat.2019.121030.
[35] Z. Du, S. Deng, Y. Chen, B. Wang, J. Huang, Y. Wang, G. Yu, Removal of perfluorinated carboxylates from washing wastewater of perfluorooctanesulfonyl fluoride using activated carbons and resins, J. Hazard. Mater. 286 (2015) 136–143, https://doi.org/10.1016/j.jhazmat.2014.12.037.
[36] C. Fu, X. Xu, C. Zheng, X. Liu, D. Zhao, W. Qiu, Photocatalysis of aqueous PFOA by common catalysts of In(2)O(3), Ga(2)O(3), TiO(2), CeO(2) and CdS: influence factors and mechanistic insights, Environ. Geochem. Health 44 (9) (2022) 2943–2953, https://doi.org/10.1007/s10653-021-01127-2.
[37] B. Zhao, M. Lv, L. Zhou, Photocatalytic degradation of perfluorooctanoic acid with beta-Ga2O3 in anoxic aqueous solution, J. Environ. Sci. (China) 24 (4) (2012) 774–780, https://doi.org/10.1016/s1001-0742(11)60818-8.
[38] Y. Yuan, L. Feng, X. He, X. Liu, N. Xie, Z. Ai, L. Zhang, J. Gong, Efficient removal of PFOA with an In(2)O(3)/persulfate system under solar light via the combined process of surface radicals and photogenerated holes, J. Hazard. Mater. 423 (Pt B) (2022) 127176, https://doi.org/10.1016/j.jhazmat.2021.127176.
[39] Z. Li, P. Zhang, J. Li, T. Shao, J. Wang, L. Jin, Synthesis of In2O3 porous nanoplates for photocatalytic decomposition of perfluorooctanoic acid (PFOA), Catal. Commun. 43 (2014) 42–46, https://doi.org/10.1016/j.catcom.2013.09.004.
[40] Z. Wan, Q. Mao, Q. Chen, Proton-dependent photocatalytic dehalogenation activities caused by oxygen vacancies of In2O3, Chem. Eng. J. 403 (2021), https://doi.org/10.1016/j.cej.2020.126389.
[41] Z. Li, P. Zhang, T. Shao, X. Li, In2O3 nanoporous nanosphere: a highly efficient photocatalyst for decomposition of perfluorooctanoic acid, Appl. Catal. B 125 (2012) 350–357, https://doi.org/10.1016/j.apcatb.2012.06.017.
[42] X. Gao, J. Chen, H. Che, Y. Ao, P. Wang, Surface complex and nonradical pathways contributing to high-efficiency degradation of perfluorooctanoic acid on oxygen-deficient In2O3 derived from an in-based metal organic framework, ACS ES&T Water 2 (8) (2022) 1344–1352, https://doi.org/10.1021/acsestwater.2c00078.
[43] F. Jiang, H. Zhao, H. Chen, C. Xu, J. Chen, Enhancement of photocatalytic decomposition of perfluorooctanoic acid on CeO2/In2O3, RSC Adv. 6 (76) (2016) 72015–72021, https://doi.org/10.1039/c6ra09856h.
[44] W. Zhang, H. Efstathiadis, L. Li, Y. Liang, Environmental factors affecting degradation of perfluorooctanoic acid (PFOA) by In(2)O(3) nanoparticles, J. Environ. Sci. (China) 93 (2020) 48–56, https://doi.org/10.1016/j.jes.2020.02.028.
[45] X. Li, P. Zhang, L. Jin, T. Shao, Z. Li, J. Cao, Efficient photocatalytic decomposition of perfluorooctanoic acid by indium oxide and its mechanism, Environ. Sci. Tech. 46 (10) (2012) 5528–5534, https://doi.org/10.1021/es204279u.
[46] Y. Wu, Y. Li, C. Fang, C. Li, Highly efficient degradation of perfluorooctanoic acid over a MnOx -modified oxygen-vacancy-rich In2O3 photocatalyst, ChemCatChem 11 (9) (2019) 2297–2303, https://doi.org/10.1002/cctc.201900273.
[47] C. Xu, P. Qiu, H. Chen, F. Jiang, Platinum modified indium oxide nanorods with enhanced photocatalytic activity on degradation of perfluorooctanoic acid (PFOA), J. Taiwan Inst. Chem. Eng. 80 (2017) 761–768, https://doi.org/10.1016/j.jtice.2017.09.018.
[48] X. Liu, X. Duan, T. Bao, D. Hao, Z. Chen, W. Wei, D. Wang, S. Wang, B.J. Ni, High-performance photocatalytic decomposition of PFOA by BiOX/TiO(2) heterojunctions: Self-induced inner electric fields and band alignment, J. Hazard. Mater. 430 (2022) 128195, https://doi.org/10.1016/j.jhazmat.2021.128195.
[49] Z. Warren, T. Tasso Guaraldo, A.S. Martins, J. Wenk, D. Mattia, Photocatalytic foams for water treatment: a systematic review and meta-analysis, J. Environ. Chem. Eng. 11 (1) (2023) 109238, https://doi.org/10.1016/j.jece.2022.109238.
[50] S. Horikoshi, N. Serpone, Can the photocatalyst TiO2 be incorporated into a wastewater treatment method? background and prospects, Catal. Today 340 (2020) 334–346, https://doi.org/10.1016/j.cattod.2018.10.020.
[51] J.C. Espíndola, R.O. Cristóvão, A. Mendes, R.A.R. Boaventura, V.J.P. Vilar, Photocatalytic membrane reactor performance towards oxytetracycline removal from synthetic and real matrices: Suspended vs immobilized TiO2-P25, Chem. Eng. J. 378 (2019), https://doi.org/10.1016/j.cej.2019.122114.
[52] N. Kaishubayeva, C. Ponce de León, F.C. Walsh, L.F. Arenas, Design, imaging and performance of 3D printed open-cell architectures for porous electrodes: quantification of surface area and permeability, J. Chem. Technol. Biotechnol. 96 (7) (2021) 1818–1831, https://doi.org/10.1002/jctb.6754.

[53] D.W. Yee, M.L. Lifson, B.W. Edwards, J.R. Greer, Additive Manufacturing of 3D-Architected Multifunctional Metal Oxides, Adv. Mater. 31 (33) (2019) e1901345.
[54] H. Dommati, S.S. Ray, J.C. Wang, S.S. Chen, A comprehensive review of recent developments in 3D printing technique for ceramic membrane fabrication for water purification, RSC Adv. 9 (29) (2019) 16869–16883, https://doi.org/10.1039/c9ra00872a.
[55] T.T. Guaraldo, R. Vakili, J. Wenk, D. Mattia, Highly efficient ZnO photocatalytic foam reactors for micropollutant degradation, Chem. Eng. J. 455 (2023), https://doi.org/10.1016/j.cej.2022.140784.
[56] X. Lei, L. Yao, Q. Lian, X. Zhang, T. Wang, W. Holmes, G. Ding, D.D. Gang, M. E. Zappi, Enhanced adsorption of perfluorooctanoate (PFOA) onto low oxygen content ordered mesoporous carbon (OMC): Adsorption behaviors and mechanisms, J. Hazard. Mater. 421 (2022) 126810, https://doi.org/10.1016/j.jhazmat.2021.126810.
[57] S.S. Elanchezhiyan, J. Preethi, K. Rathinam, L.K. Njaramba, C.M. Park, Synthesis of magnetic chitosan biopolymeric spheres and their adsorption performances for PFOA and PFOS from aqueous environment, Carbohydr. Polym. 267 (2021) 118165, https://doi.org/10.1016/j.carbpol.2021.118165.
[58] X. Liu, Z. Chen, K. Tian, F. Zhu, D. Hao, D. Cheng, W. Wei, L. Zhang, B.-J. Ni, Fe3+ Promoted the Photocatalytic Defluorination of Perfluorooctanoic Acid (PFOA) over In2O3, ACS ES&T Water 1 (11) (2021) 2431–2439, https://doi.org/10.1021/acsestwater.1c00275.
[59] Z. Warren, T.T. Guaraldo, J. Wenk, D. Mattia, Synthesis of photocatalytic pore size-tuned ZnO molecular foams, J. Mater. Chem. A 10 (21) (2022) 11542–11552, https://doi.org/10.1039/d2ta02038f.
[60] S. Deng, Q. Zhang, Y. Nie, H. Wei, B. Wang, J. Huang, G. Yu, B. Xing, Sorption mechanisms of perfluorinated compounds on carbon nanotubes, Environ. Pollut. 168 (2012) 138–144, https://doi.org/10.1016/j.envpol.2012.03.048.
[61] Z. Zhang, D. Sarkar, R. Datta, Y. Deng, Adsorption of perfluorooctanoic acid (PFOA) and perfluorooctanesulfonic acid (PFOS) by aluminum-based drinking water treatment residuals, Journal of Hazardous Materials Letters 2 (2021), https://doi.org/10.1016/j.hazl.2021.100034.
[62] N. Gevaerd de Souza, A.C. Parenky, H.H. Nguyen, J. Jeon, H. Choi, Removal of perfluoroalkyl and polyfluoroalkyl substances in water and water/soil slurry using Fe(0) -modified reactive activated carbon conjugated with persulfate, Water Environ. Res 94 (1) (2022) e1671.
[63] M. Ateia, M.F. Attia, A. Maroli, N. Tharayil, F. Alexis, D.C. Whitehead, T. Karanfil, Rapid removal of poly- and perfluorinated alkyl substances by poly(ethylenimine)-functionalized cellulose microcrystals at environmentally relevant conditions, Environ. Sci. Technol. Lett. 5 (12) (2018) 764–769, https://doi.org/10.1021/acs.estlett.8b00556.
[64] F. Cao, L. Wang, X. Ren, H. Sun, Synthesis of a perfluorooctanoic acid molecularly imprinted polymer for the selective removal of perfluorooctanoic acid in an aqueous environment, J. Appl. Polym. Sci. 133 (15) (2016), https://doi.org/10.1002/app.43192.
[65] F. Wang, K. Shih, Adsorption of perfluorooctanesulfonate (PFOS) and perfluorooctanoate (PFOA) on alumina: influence of solution pH and cations, Water Res. 45 (9) (2011) 2925–2930, https://doi.org/10.1016/j.watres.2011.03.007.
[66] F. Wang, C. Liu, K. Shih, Adsorption behavior of perfluorooctanesulfonate (PFOS) and perfluorooctanoate (PFOA) on boehmite, Chemosphere 89 (8) (2012) 1009–1014, https://doi.org/10.1016/j.chemosphere.2012.06.071.
[67] C. Zhu, J. Xu, S. Song, J. Wang, Y. Li, R. Liu, Y. Shen, TiO(2) quantum dots loaded sulfonated graphene aerogel for effective adsorption-photocatalysis of PFOA, Sci. Total Environ. 698 (2020) 134275, https://doi.org/10.1016/j.scitotenv.2019.134275.
[68] Z. Kong, L. Lu, C. Zhu, J. Xu, Q. Fang, R. Liu, Y. Shen, Enhanced adsorption and photocatalytic removal of PFOA from water by F-functionalized MOF with in-situ-growth TiO2: Regulation of electron density and bandgap, Sep. Purif. Technol. 297 (2022), https://doi.org/10.1016/j.seppur.2022.121449.
[69] S. Kundu, S. Patel, P. Halder, T. Patel, M. Hedayati Marzbali, B.K. Pramanik, J. Paz-Ferreiro, C.C. de Figueiredo, D. Bergmann, A. Surapaneni, M. Megharaj, K. Shah, Removal of PFASs from biosolids using a semi-pilot scale pyrolysis reactor and the application of biosolids derived biochar for the removal of PFASs from contaminated water, Environ.. Sci.: Water Res. Technol. 7 (3) (2021) 638–649, https://doi.org/10.1039/d0ew00763c.